Modeling and Testing of Phase Transition-Based Deployable Systems for Small Body Sample Capture

Marco Quadrelli[1], Paul Backes[2], Keats Wilkie[3], Lou Giersch[4],
Ubaldo Quijano[5], Jason Keim[6], Rudranarayan Mukherjee[7]
Jet Propulsion Laboratory, California Institute of Technology, 4800 Oak Grove Drive, Pasadena, CA 91109-8099

This paper summarizes the modeling, simulation, and testing work related to the development of technology to investigate the potential that shape memory actuation has to provide mechanically simple and affordable solutions for delivering assets to a surface and for sample capture and return. We investigate the structural dynamics and controllability aspects of an adaptive beam carrying an end-effector which, by changing equilibrium phases is able to actively decouple the end-effector dynamics from the spacecraft dynamics during the surface contact phase. Asset delivery and sample capture and return are at the heart of several emerging potential missions to small bodies, such as asteroids and comets, and to the surface of large bodies, such as Titan.

Nomenclature

c = specific heat of material
E_M , E_A = elastic moduli of martensite and austenite, respectively.
E_{eff} = effective Young's modulus of the SMA material.
f = contact force
j = electric current
x_A, x_+, x φ = phase fractions
p^{+A}= transition probability from M+ phase to A phase
q = physical displacements
S_V = surface area to volume ratio
S_A, S_M , S_{eff} = effective electrical conductivity
T = material temperature
T_0 = temperature of environment
α = convection heat transfer coefficient
α_A, α_M, α_{eff} = coefficient of thermal expansion (CTE) of the SMA material
ε = mechanical strain,
ε_0 = maximum recoverable quasiplastic residual strain
ε^t = phase transition strain within the SMA material
ρ = material density
ξ = instantaneous martensite volume fraction within the material
σ = uni-axial stress

[1] Corresponding author, Senior Engineer, Mail Stop 198-326, Guidance and Control Analysis Group, , Marco.B.Quadrelli@jpl.nasa.gov, senior AIAA member
[2] Principal Engineer, Sample Acquisition and Handling Group
[3] Senior Engineer, Advanced Deployable Structures Group
[4] Staff Engineer, Deployable Structures Group
[5] Associate Staff Engineer, Deployable Structures Group,
[6] Staff Engineer, Guidance and Control Analysis Group
[7] Senior Engineer, Sample Acquisition and Handling Group

I. Introduction

In this paper, we investigate the structural dynamics and controllability aspects of an adaptive beam carrying an end-effector which, changing equilibrium phases is able to actively decouple the end-effector dynamics from the spacecraft dynamics during the surface contact phase. Asset delivery and sample capture and return are at the heart of several emerging potential missions to small bodies, such as asteroids, and to the surface of large bodies, such as Titan. The objective of this research is to investigate the potential that shape memory actuation has to provide mechanically simple and affordable solutions for delivering assets to a surface and for sample capture and return.

Shape memory materials (SMA) possess an interesting property by which the material remembers its original size or shape and reverts to it at a characteristic phase transformation temperature. By training an SMA wire to remember a given straight or curved shape when heated or cooled down to a given temperature, a long wire with low inherent bending stiffness may be ejected or unreeled from a spacecraft and then transformed into a long thin beam via a controlled material phase transition. Once the phase transition has been induced, the wire exhibits a bending stiffness that did not exist before, and the deployed appendage operates now as a stiff robotic arm. Figure 1 shows a conceptual view of how artificial manipulator tensioning would occur via an embedded SM wire, and a proposed sequence for sample capture phase. Conversely, when the phase transition reverses, the original state of string behavior dominated by axial tension is recovered and the appendage can be reeled back inside the spacecraft. The transition is almost perfectly reversible and, in principle, many cycles can be performed reliably, which enables either deployment of an asset or retrieval of a collected sample. Shape memory phase transition behavior is tailorable, and compositions exist that have been tested at –99 degrees C and below. After plastic deformation at low temperature, the SMA returns to its original configuration upon the supply of heat. The material seems to remember its former shape, which gives the name to the effect. At a higher temperature, another important phenomenon can be observed. Here, the material can be reversibly deformed up to 10% of its original length under a nearly constant load—this behavior is termed superelasticity. Both effects are a consequence of the load-deformation behavior, which is called quasiplastic at low temperature and pseudoelastic at higher temperature. The underlying mechanism of the observed phenomena is a phase transformation between different crystallographic structures, i.e. different variants of the martensite and the austenite phases. A variety of asset deployment of sample capture scenarios would be possible that could potentially minimize the dynamic interactions with the spacecraft during the maneuver. For example, a minimum load of 20 N was shown to be required to be maintained on the end-effector for approximately 2 seconds so that enough soil sample could be collected from an asteroid, which translated in an adverse reaction on the spacecraft and necessitated additional use of the thrusters to correct the attitude at the end of the maneuver. With the new concept, the stiffness of the end-effector arm can be actively modulated so that the back-reaction on the spacecraft can be greatly reduced. Since the rigidity of the link can now be tailored electrically to specific values, innovative scenarios involving different end-effectors can be envisioned that are highly repeatable, simpler in design, with lower mass, power, and cost.

Consequently, we have synthesized the following problem statement: given the spacecraft, manipulator, and terrain models, develop an adaptive control logic and actuator location distribution for the manipulator stiffness that, in conjunction with the attitude and altitude control of the vehicle, decouples the dynamics of the spacecraft from the dynamics of the end-effector while collecting a sample, in a stable manner over a specified amount of time. The adaptive control law is such that the curvature of the manipulator can be modulated over the time the sample has to be collected.

The paper approaches this complex problem sequentially. The first step is the static and dynamic characterization of the component behavior of a shape memory element. The second step is to investigate the system-level characteristics of the problem, in reference to the touch-and-go maneuver that would be necessary for sample collection. In each step, we have followed an analysis phase in conjunction with a testing phase. Hence, a test-model correlation step is also necessary at each step. In this paper, we describe these initial, albeit necessary steps, before we tackle the more complex problem of closing a control loop around this system.

Section II discusses the coupled Electro-Thermal-Mechanical modeling of shape memory alloy elements. Section III describes the system-level dynamics simulation of the touch-and-go scenario. Section IV describes the hardware tests and model correlation study. Section V provides the conclusion of the paper.

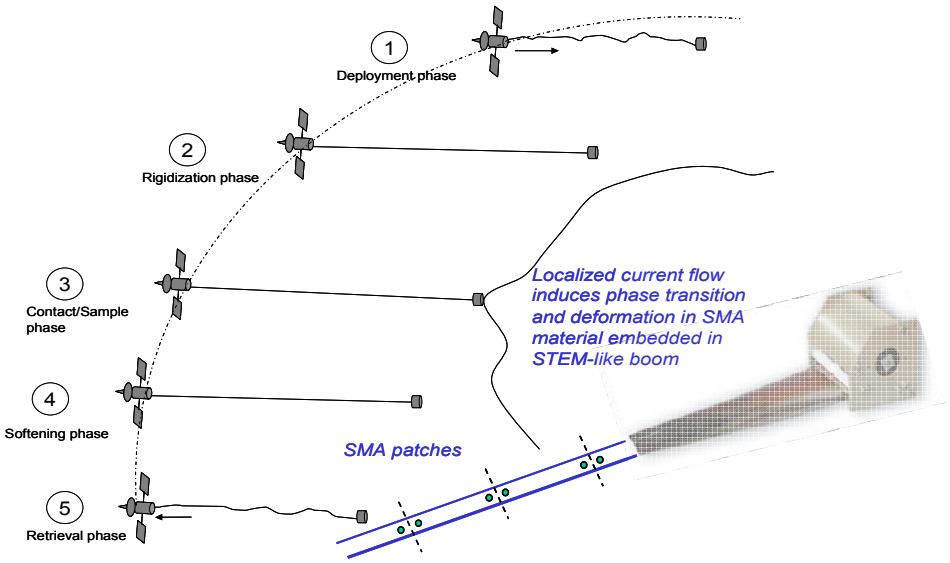

Figure 1. Scenario of Application

II. Coupled Electro-Thermal-Mechanical Modeling of Shape Memory Alloy Elements

In our integrated vehicle dynamics model, we assume that the spacecraft exhibits in-plane dynamics only (3 degrees of freedom), and that it is a rigid spacecraft (no flexibility). The end effector is assumed to contact the surface of the body for a specific duration of time (dwell time), during which the specific mechanics of the sampler device enables the material collection and transmits a horizontal and vertical force to the spacecraft-sampler system. The contact force components are proportional to the horizontal and vertical components of the velocity of the end effector through the static and dynamic friction coefficients of the surface. The manipulator is assumed to act as a massless axial spring that behaves hysteretically, and the properties of the spring are controllable. In the model, we also assume that we can measure the position and attitude of the spacecraft, and that we can measure the contact force. Figure 2 also shows the initial configuration of our multibody dynamics simulation, a system of 10 bodies and 9 rigid links actuated by springs. Summarizing the above assumptions in analytic form, the physics of the system is described by a structural dynamics equation of motion for the physical displacements q in the second order ODE form $M(q)\ddot{q}+C(q,\dot{q})\dot{q}+K(q)q=f(q,\dot{q},t)$, a phase transition balance equation for the phases φ ($\dot{\varphi}=g(\varphi,\sigma,T)$, where σ is the stress on the axial member), and T is the temperature, a thermal balance equation ($\dot{T}=h(T,\varphi,j)$, where j is the current), and the set of initial conditions $q(0)=q_0,\dot{q}(0)=\dot{q}_0,T(0)=T_0,\varphi(0)=\varphi_0$. The actuation inputs are the contact force *f,* the temperature T, and the current j. In conclusion, for a given applies stress and Joule heat, we can evaluate the phase fractions and the temperature by integrating the system of equations simultaneously, and then calculate the resulting strain. Alternatively, by prescribing strain and Joule heat, we can compute the phase fractions, temperature, and stress.

To achieve the full potential of shape memory actuation, it is necessary to develop models that characterize the hysteretic nonlinearities inherent in the constituent materials. Additionally, the design of SMA actuators necessitates the development of control algorithms based on those models. We have investigated models that quantify the nonlinearities and hysteresis inherent to phase transition, each in formulations suitable for subsequent control design. Candidate models that have been proposed in the past employ either domain theory to quantify phase transition behavior under isothermal conditions[2,4], or a Muller-Achenbach-Seelecke[10] framework, where a transition state theory of non-equilibrium processes is used to derive rate laws for the evolution of material phase fractions. These models involve first-order, nonlinear ordinary differential equations and require few parameters that are readily identifiable from measurements, hence we have selected to use these differential models in our analysis (see Figure 2 for a simulation of pseudoelastic phase transition behavior).

A. Muller-Achenbach-Seelecke[10] Model

The explicit stress-strain relationship can be derived as follows:

$$\sigma(\varepsilon) = \frac{E_M[\varepsilon - (x_+ - x_-)\varepsilon_0]}{x_+ + x_- + \frac{E_M}{E_A} x_A} \tag{1}$$

The maximum recoverable quasiplastic residual strain ε_0 can be identified from experiment. The evolution of the phase fractions x_A, x_+, x_- is governed by the rate laws:

$$\begin{aligned} \dot{x}_+ &= -x_+ p^{+A} + x_A p^{A+} \\ \dot{x}_- &= -x_- p^{-A} + x_A p^{A-} \end{aligned} \tag{2}$$

where the homogeneity law $x_A + x_- + x_+ = 1$ holds. The quantities in the rates of the phase fractions are transition probabilities, for example, p^{+A} is the transition probability from M+ phase to A phase. The transition probabilities are computed as the product of the probability of achieving the energy required to overcome the energy barrier and the frequency at which jumps are tempted. SMA actuators are typically driven by electric current heating. The temperature change coupled with the mechanical loading triggers the phase transformation between martensite and austenite, and generates the material deformation. Assuming uniform temperature changes through the material, the heat transfer equation becomes:

$$\rho c \dot{T} = -\alpha S_V (T - T_0) - \sigma_R \varepsilon_R (T^4 - T_0^4) + j(t) - (h_{M+} - h_A)\dot{x}_+ - (h_{M-} - h_A)\dot{x}_- \tag{3}$$

where the specific heat c is assumed to be the same for the austenite and martensite phases. The first term is the heat convection to the environment with temperature T_0. The third term is the heat exchanged with the environment by radiation. The fourth term is the Joule heating. The last two terms represent the rate dependent heat generation and loss due to the phase transformation, where the *h*-terms represent the latent heats of transformation of each phase.

The hysteretic constitutive model has been tested numerically under axial loading and thermal input in Matlab® and COMSOL®. The model combines the thermo-electromechanical elements of the SMA behavior in an integrated multi-physics simulation environment (electromagnetic, thermal, mechanical). Simulated pseudo-elastic behavior of SMA tested with the Muller-Achenbach-Seelecke model is shown in Figure 2.

B. Dano-Hyer[2,4] Model

A simple, two-phase phase kinetics model was utilized to represent the material transition behavior of a shape memory alloy filament subject acting under a constant, static tensile load. The phase kinetics model is adapted from one used by Dano and Hyer[2], the thermodynamics of which were developed by Boyd and Lagoudas[4]. The fundamental constitutive equation used for the SMA material element is a modified Hooke's law

$$\sigma = E_{eff}\varepsilon^e = E_{eff}\left(\varepsilon - \varepsilon^t - \alpha_{eff}\left(T - T_0\right)\right) \tag{4}$$

This transformation strain is defined as

$$\varepsilon^t = \varepsilon_0 \xi \tag{5}$$

The martensite volume fraction is itself a function of stress and temperature. For transitions occurring under static loading, it may be solved for directly as a function of temperature using the modified Gibbs free energy relation

$$\xi = \xi\left(T, \sigma_{stat}\right) = \left(\sigma_{stat}\varepsilon_0 + \tfrac{1}{2}\Delta a^1 \sigma_{stat}^2 + \Delta\alpha\sigma_{stat}\left(T - T_0\right) + \rho\Delta a^4 T - Y\right) \Big/ \rho b^1 \qquad (6)$$

This relationship is valid only in the transition temperature region between $A_s<T<A_f$, for martensite to austenite transitions, and $M_f<T<M_s$ for austenite to martensite transitions. These transition temperatures are generally functions of stress within the material. A graphical representation of martensite volume fraction as a function of stress and temperature is shown in Figure 3.

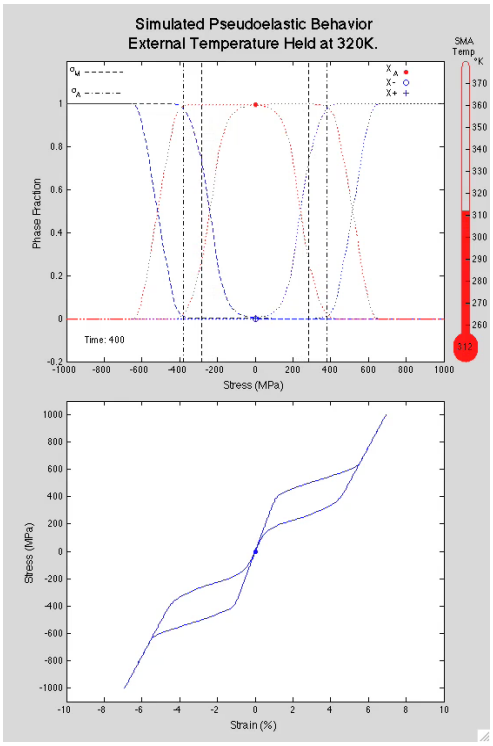

Figure 2. Simulated Pseudo-elastic behavior of SMA tested with the Muller-Achenbach-Seelecke Model.

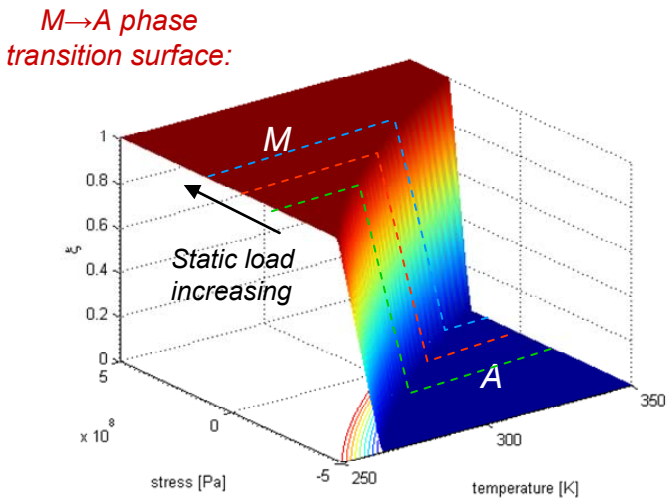

Figure 3. Schematic representation of the martensite to austenite transition surface for ξ, defined by Eq. 3. The martensite volume fraction, ξ, is a function of stress and temperature.

These parameters, as well as effective electrical conductivity, S_{eff}, used in the Joule heating calculations, are determined using simple rules-of-mixtures relations between the instantaneous martensite and austenite volume fractions within the material:

$$\begin{aligned} E_{eff} &= E_A + \xi\left(E_M - E_A\right) \\ \alpha_{eff} &= \alpha_A + \xi\left(\alpha_M - \alpha_A\right) \\ S_{eff} &= S_A + \zeta\left(S_M - S_A\right) \end{aligned} \tag{7}$$

Designing a shape-memory alloy-actuated sample acquisition structure will require an analytical framework capable of modeling the interactions between thermo-elastic mechanics and the material phase transition behavior. For this effort, we have adopted the *COMSOL Multiphysics*[3] computational analysis package for this purpose. COMSOL features discipline-specific physics modules that can be coupled, as needed, at the partial differential equation level. For the simple SMA actuators examined here, the core physics and their primary interactions are modeled using the structural mechanics, heat transfer, and AC/DC modules. To this analytical foundation, a simple two-phase material kinetics model was added. A description of the complete model, developed for exploring the SMA analytical capability of COMSOL, is described below. Correlation of analytical results with a series of simple experiments, designed to identify key material parameters for the SMA materials used throughout this study, are also presented. Values for these and remaining SMA material constants used in Eq. 6 are given in Table I.

Table I. Shape memory alloy material properties used for COMSOL analysis

symbol	*value/expression*	*description*
E_A	41 [GPa]	Young's modulus, austenite phase
E_M	28 [GPa]	Young's modulus, martensite phase
α_A	11e-6 [1/K]	CTE, austenite
α_M	6.6e-6 [1/K]	CTE, martensite
S_A	1.2e6 [S/m]	Electrical conductivity, austenite
S_M	1.3e6 [S/m]	Electrical conductivity, martensite
A_s	302 [K]	Austenite transition, start temperature
A_f	307 [K]	Austenite transition, finish temperature
M_s	289 [K]	Martensite transition, start temperature
M_f	284 [K]	Martensite transition, finish temperature
ε_0	0.047 [-]	Maximum recoverable plastic strain
ρ	6500 [kg/m^3]	SMA material density
T_0	293.15 [K]	Material properties reference temperature
C_A	41.3e6 [Pa/K]	Critical stress-temperature slope, $M \rightarrow A$
C_M	12.4e6 [Pa/K]	Critical stress-temperature slope, $A \rightarrow M$
k	18 [W/m/K]	SMA nominal thermal conductivity
C_p	600 [J/kg/K]	SMA nominal specific heat
e	0.8 [-]	SMA nominal surface emissivity
h	150 [W/m^2/K]	Surface heat transfer coefficient, SMA→ambient
Δa^1	$1/E_M - 1/E_A$	Martensite-austenite compliance difference
Δa^4 $(M \rightarrow A)$	$-C_A\varepsilon_0/\rho$	Specific entropy, $M \rightarrow A$
Δa^4 $(A \rightarrow M)$	$-C_M\varepsilon_0/\rho$	Specific entropy, $A \rightarrow M$
$\Delta\alpha$	$\alpha_M - \alpha_A$	Martensite-austenite CTE difference
b^1 $(M \rightarrow A)$	$-\Delta a^4 (A_f - A_s)$	Isotropic hardening parameter, $M \rightarrow A$
b^1 $(A \rightarrow M)$	$-\Delta a^4 (M_s - M_f)$	Isotropic hardening parameter, $A \rightarrow M$
Y $(M \rightarrow A)$	$\rho\Delta a^4 A_f$	Latent heat of transformation, $M \rightarrow A$
Y $(A \rightarrow M)$	$\rho\Delta a^4 M_s$	Latent heat of transformation, $A \rightarrow M$

III. Dynamics simulation of touch-and-go scenario

A multibody dynamics simulation of the system behavior of the entire vehicle during sample capture has been developed and tested. The objective of the system model is to simulate the zero-gravity planar system-level behavior of the touch-and-go phase of a SC with an attached end-effector at the tip of a long slender boom. The touch-and-go phase involves the end effector approaching a surface, establishing contact with it, and departing from it. A description of the testbed that is being used to test the system behavior is shown in Figure 4.

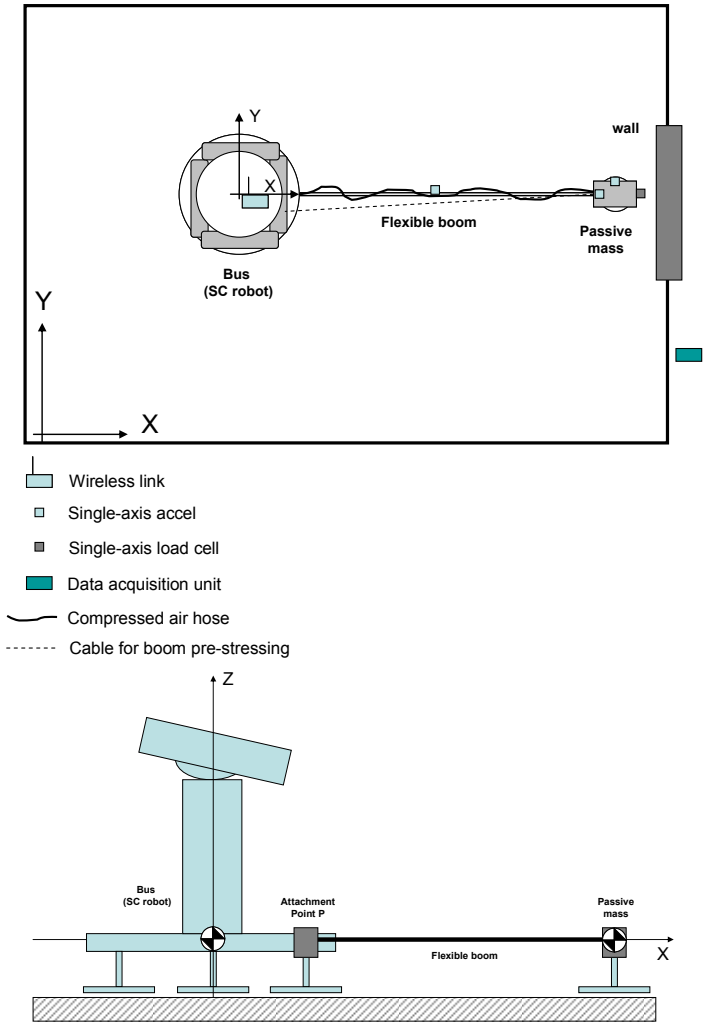

Figure 4. Top: Sketch of test to be done in space simulator. Bottom: X-Z view of test article on floor.

The tests will be carried out in the Formation Control Testbed (FCT) at JPL starting in February '09. Boom deployment will not be considered as the flexible manipulator (boom) is already deployed. Sample retrieval and handling is also not a concern at this stage. The test will provide insight into the feasibility of having a slender flexible manipulator for touch-and-go sampling. We will collect time series data of system level response at low bandwidth (0.8 Hz) using videogrammetry (for boom deflections), and at high bandwidth (> 10 Hz, during the contact phase when we will measure the contact force) using accelerometers and the load cell. This data will be used to correlate the results with those obtained with the analytical multibody model of the system.

To investigate the dynamic response of the testbed at the system level, a simulation has been carried out. The simulation study provides an insight on the stability of the system during and after contact. The simulation runs will

be done to size the system to be tested in the FCT, and the results will later be used to make a demonstration video of the touch-and-go phase. The simulation scenario contemplates a planar (2-D) system so that gravity effects are not present. Other assumptions are: rigid spacecraft body, rigid end-effector with fixed mass, flexible boom, Coulomb friction during contact, no spacecraft ACS (i.e. turned off).

A parametric study has been conducted predicting SC body rates, velocity and acceleration components as a function of: boom stiffness values (EI), contact forces, durations of contact, surface slopes, surface friction coefficients, SC horizontal and vertical component of approach velocity. The boom attachment to the base of the SC will vary as we design the bracket that attaches the boom. Some other parameters may vary as well, depending of how we scale the system configuration to fit in the FCT. Tables II-IV show the parameters that we use for the simulation. These preliminary simulation studies do not yet include the SMA model described elsewhere in this paper. The SMA model will be implemented in future studies in conjunction with the development of the force control algorithm.

For these preliminary simulation studies, Figure 5 shows the initial geometry of the multibody system, as well as a snapshot of the geometry during contact at 4 seconds. Figure 6 shows the horizontal and vertical components of the contact force as a function of the approach vertical and lateral velocities. Figure 7 shows the horizontal and vertical components of the spacecraft angular velocity as a function of the approach vertical and lateral velocities.

Table II. System mass and configuration properties (X and Y on floor, Z upwards).

Property	Value
Bus Mass [kg]	374.35
Bus moments of inertia about center of mass [kg m2]	34.7347 -0.5298 -0.0300 -0.5298 38.6601 0.8122 -0.0300 0.8122 53.6707
Location of center of mass of Bus above ground [m]	0.291
End-effector (BWS) mass [kg]	30
Bus CM to Boom attachment offset (P) along X [m]	[0.2:0.4]
Bus CM to Boom attachment offset (P) along Z [m]	[-0.2:0.2]

Table III. Sampler-terrain contact interaction parameters.

Property	Value
Range of vertical approach velocity [m/s] along X	[0.1: 0.5]
Range of horizontal approach velocity [m/s] along Y	[-0.1:0.1]
Contact spring stiffness coefficient [N/m]	[1.0:2.0]e4
Contact damper damping coefficient [Ns/m]	[1e1:1e3]
ACS control parameters	Off
Surface slope	[0°:30°]
Surface dynamic friction coefficient	[0.0:1.0]
Duration of contact [s]	[2.0:5.0]
Contact force [N]	[20:30]
SC ascent thrust applied after contact [N]	100
Force sensed by load cell to trigger ascent thruster [N]	5

Table IV. Flexible boom parameters.

Property	Value
Mass per unit length [kg/m]	[0.2:0.5]
Length [m]	3
Boom material	Aluminum
Young's modulus [N/m2]	70e9
Bending strength EI [N m2]	[100:800]
Structural damping ratio (% of critical)	0.2

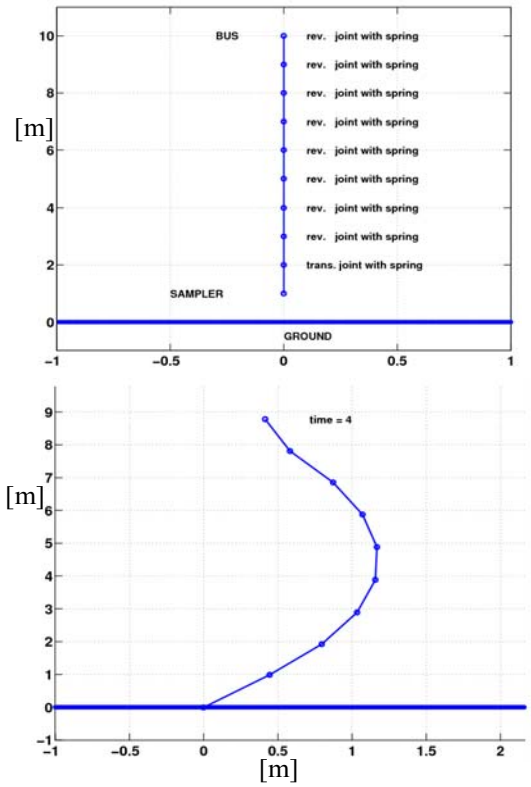

Figure 5. Snapshot of multibody dynamics simulation.

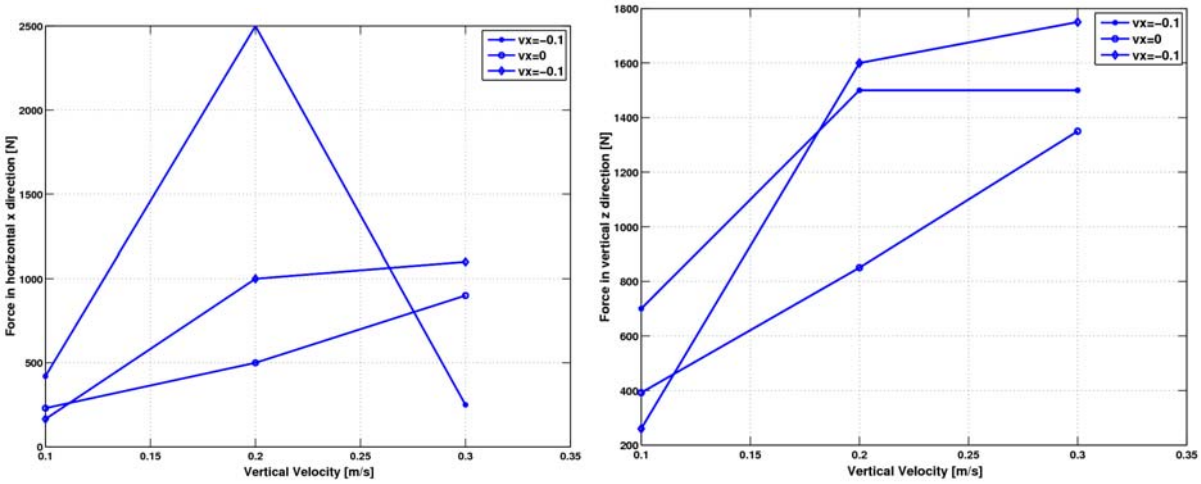

Figure 6. Horizontal and vertical contact forces as a function of approach vertical and lateral velocities.

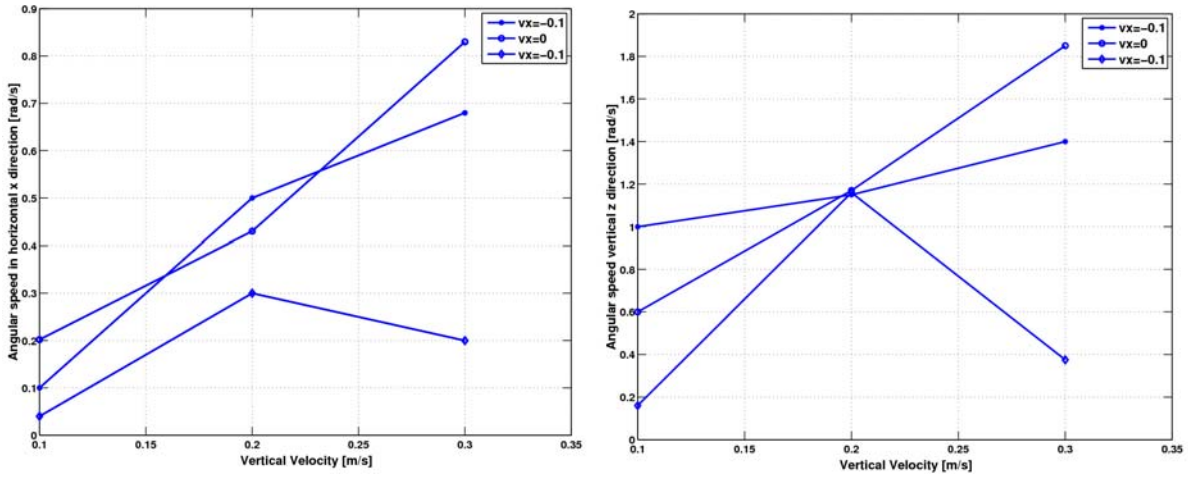

Figure 7. Horizontal and vertical components of the spacecraft angular rate as a function of approach vertical and lateral velocities.

IV. Hardware Tests

Proof-of-concept hardware was also developed and experiments were performed to demonstrate the fundamental aspects of various SMA deployable structures. These included the bonding of SMA wire to a conceptual STEM boom to demonstrate stiffening of the integrated system, and the Deployable Flexible Segment (DeFS) boom. Experimental testing and demonstration was conducted using optical diagnostics. These included the use of thermal imaging cameras to quantitatively measure the temperatures of the SMA and surrounding structure as well as digital video recorders to qualitatively measure changes in the shape of the proof-of-concept hardware. The DeFS boom was mounted vertically to demonstrate the load conditions over the workspace for small body sampling applications. Quantitative measurements of the shape of the hardware using photogrammetric and/or videogrammetric measurements have also been conducted.

C. 13 mils Diameter SMA Wire Results

Figure 8 shows the 13 mils (0.3302 mm) diameter SMA wire setup. The setup consists of the SMA wire, Keyence laser head, FLIR thermo camera, Agilent DC power supply and dead weights. The SMA wire thickness measured 0.3175 mm (12.5 mils). The overall SMA wire length measured ~52.6 cm (20.7 in). The SMA wire was connected using alligator clips in series with the output of the Agilent DC power supply. The power supply was voltage controlled driven to insure a constant voltage potential along the length of the SMA wire. Several cases were performed at constant voltages of 5, 4.5, and 4 volts. As the power supply is switched on the SMA wire shrinks and the laser head shown underneath the dead weight records the deflection with respect to time. The total SMA wire shrinkage for a particular case study at 5 volts as illustrate in Figure 8 was 22.5 mm (0.885 in). For this particular case study the SMA wire pulled a combined weight of 1.14 kg (2.51 lbs). Also different case studies were performed using different dead weights. During each case study a FLIR thermo camera was used to capture the temperature gradient of the SMA wire. Figure 8 shows a snap shot of the SMA wire seen by the FLIR thermo camera. The maximum temperature the SMA wire exhibited is around 71 Celsius (160 Fahrenheit). The FLIR camera and the Keyence laser head were synchronous to obtain the temperature versus deflection characteristic plot of the SMA wire.

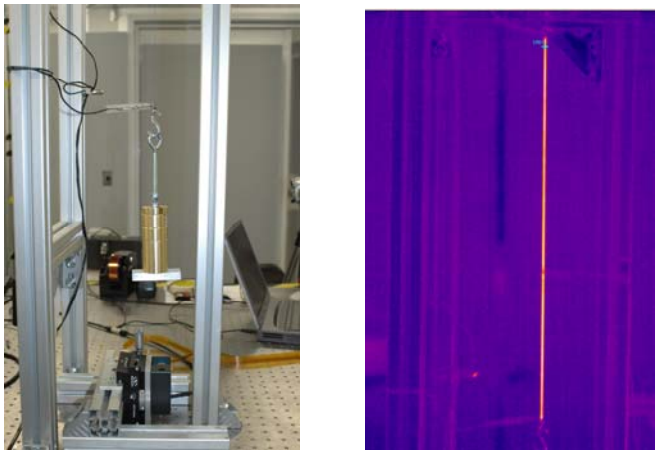

Figure 8. Left: SMA demo setup. Right: Joule heating of SMA wire as seen through thermal imaging camera.

1. SMA actuator configuration and COMSOL analysis description

A simple geometry, shown in Fig. 9, was used for investigating general SMA actuation behavior in COMSOL of the test setup depicted in Figure 8.

COMSOL 3.5a's pre-built Axial symmetry (2D) Thermal-Electric-Structural Interaction mode was used as the basis for the model. The axial strain equations were modified to include the phase transition strain, as described in Eqs. (4-6). Material modulus and CTE, now functions of the martensite volume fraction, ξ, were determined using Eq. (7). Joule heating of the element, radiative heat transfer, and simplified surface-to-ambient heat convection are represented in the couple model. COMSOL is capable of more sophisticated convective heat transfer modeling, but for simplicity, these features were not exercised here. The COMSOL 3.5a time-dependent segregated solver on default settings was used to solve the resulting coupled quasi-static, transient problem.

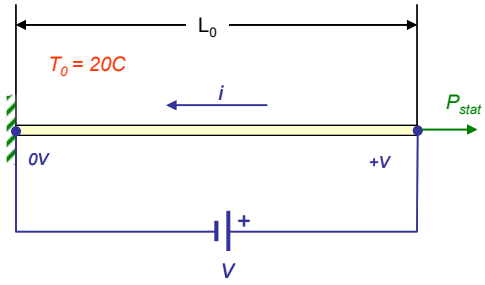

Figure 9. Simple SMA actuator geometry for COMSOL studies. The actuator consists of a thin, cylindrical SMA element of length L_0 under a constant static load, P_{stat}. A fixed voltage, V_0, is applied at one end to produce Joule heating of the SMA element.

2. Model-Test correlation

The COMSOL analysis and simple two-phase material model was able to qualitatively capture the stress and temperature dependent phase transition loop behavior after appropriate tuning of the SMA material parameters using test data. Calculated martensite-to-austenite, and reverse, austenite-to-martensite transition loops for the test geometry are shown in Figure 10 as a function of two applied static loading cases.

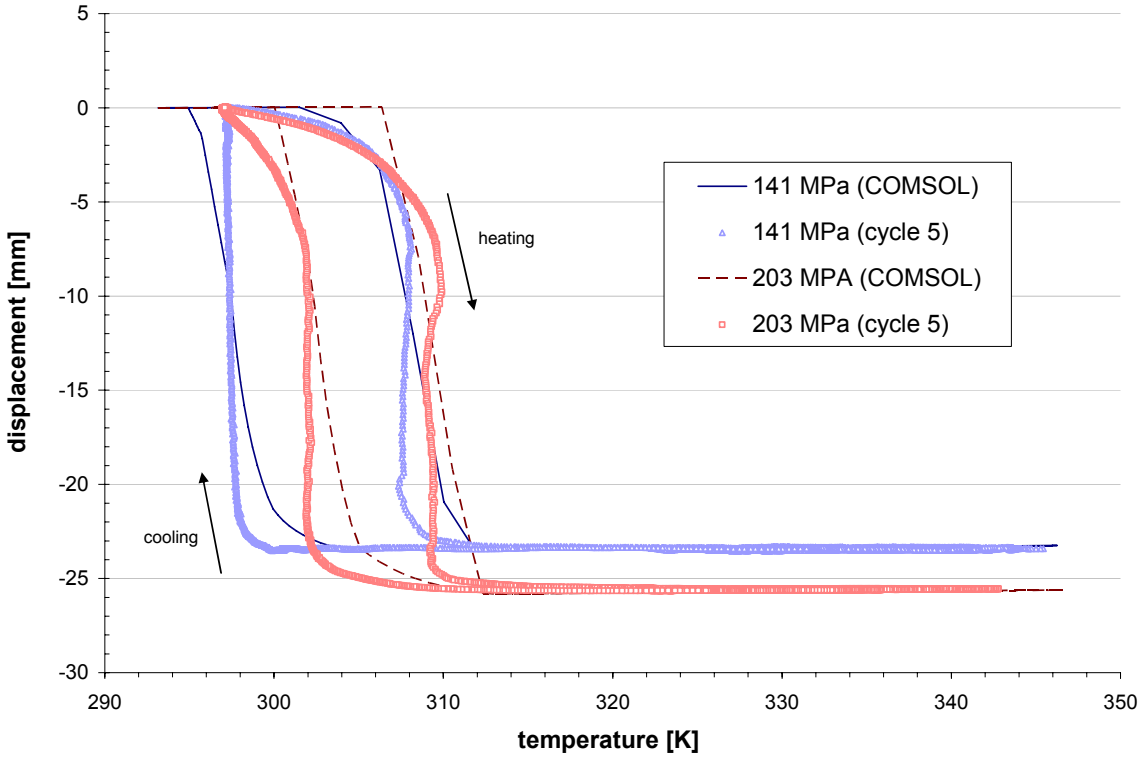

Figure 10. COMSOL predicted displacement-temperature transition loop behavior versus static stress for the test SMA actuator geometry: L_0 = 526 mm; d = 0.3175 mm. Experimental temperatures were obtained using high-speed thermal imaging of the SMA element. Displacement data was obtained using a laser displacement sensor. Sampling interval for the data shown is 0.02 seconds.

Future improvements in the analysis will incorporate a more sophisticated convective heat transfer model, which, although not present in space, will be important for correlation with laboratory test data. Better tuning of the SMA thermal properties is also in order. Finally, to be more generally useful, SMA phase transition behavior will need to be solved for non-static stress loadings, as would be the case in situations where an SMA filament is operating against a spring or elastic flexure, for example, with the Formation Flying Laboratory demonstration test article, described elsewhere in this paper.

D. Pathfinder SMA Experiment Status

A pathfinder experiment was also developed to validate and facilitate the development of the full-scale experiment shown in Figure 4. The pathfinder experiment consisted primarily of a strip of spring steel beam 1" wide, 0.012" thick, and 18" long. A wire of shape memory alloy (SMA) 0.0039" in diameter was attached to the spring steel beam with eyebolts. The SMA wire was routed along the length of the spring steel beam. The beam was then cantilevered off a test fixture (figures 11 and 12). Initial tension in the SMA wire was maintained using turnbuckles attached to the test fixture and each end of the wire, with accommodations made for electrically connecting the SMA wire to a pulsed power supply. The turnbuckles were only used to adjust the tension when the SMA wire was in the Martensite phase; the turnbuckles were not adjusted after the SMA wire was heated to the Austenite phase.

Figure 11. Top: Spring steel beam with SMA wire cantilevered off test fixture. Bottom: Top-down view of the beam and SMA wire.

The pulsed power supply consisted of a 0.074 Farad electrolytic capacitor charged to 48 V. When activated by a manual switch, the capacitor discharged through a 1 Ohm current limiting resistor and the SMA wire. The resulting joule heating of the SMA wire was sufficient to transition the SMA from the Martensite phase to the Austenite phase in less than one second. The backside of the beam and test fixture was covered in retro-reflective optical targets to facilitate photogrammetric measurements of the shape of the beam (figure 12). Photogrammetry is a measurement technique by which the three dimensional shape of an object is reconstructed from multiple photographs of the object taken from different camera locations and orientations. Under proper conditions photogrammetric measurement accuracy can exceed 1 part in 100,000.

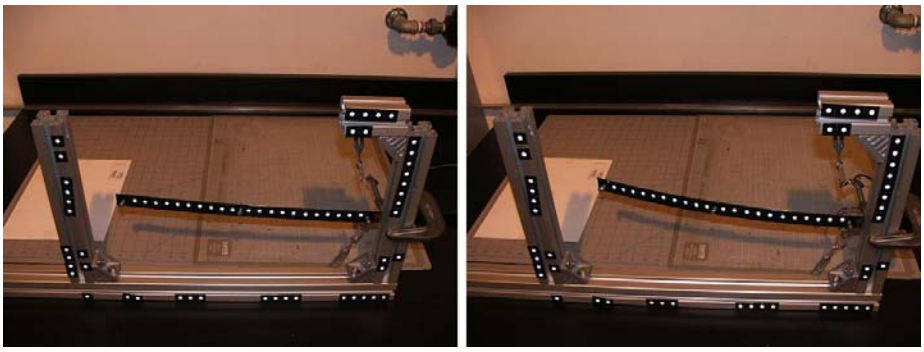

Figure 12. Typical photographs used to measure the shape of the beam with the SMA wire in the Martensite (left) and Austensite (right) phases.

Preliminary photogrammetric measurements of the beam and test fixture were made when the SMA wire was in both the Martensite (cold) and Austensite (hot) phases. Optical targets on the beam yielded data on the three-dimensional shape of the beam both before and after SMA actuation (figure 13). Optical targets on the test fixture yielded reference data and aided in camera calibration, which increased the overall accuracy of the photogrammetric measurements. Although the beam is seen to be slightly bent prior to SMA activation, the bending of the beam is markedly increased after SMA activation.

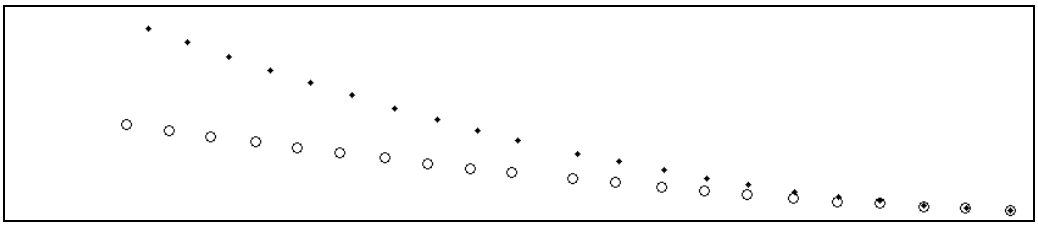

Figure 13. Data from preliminary photogrammetric measurements of the pathfinder demonstrator; 'o' is when the SMA is cold, '•' is when the SMA is hot.

E. Proof of Concept Demonstration of Sampling with a Deployable Flexible Segment Boom

Sample acquisition from a long flexible boom will also be demonstrated in a proof-of-concept test. The Deployable Flexible Segment (DeFS) boom concept is shown in Figure 14. A multi-segment flexible boom would be deployed from a spacecraft in a microgravity environment, e.g. in the proximity of a comet for a comet sampling mission. The boom end point would be controlled via tensioning of three cables between the spacecraft and the end of the boom. A sampling tool would be at the end of the boom. The boom has an active joint in the middle and the joints between the other segments might deploy only once. The cables are tensioned to bend the boom at the desired initial sampling force. The spacecraft would then approaches the small body, e.g. comet, until the sampling tool contacts the small body at which time the boom would begin to bend to accommodate the position constraint of the surface. The sampling tool would acquire the sample while the boom bends to accommodate the relative motion of the spacecraft and the small body and to provide the contact force needed for sampling by the sampling tool. The spacecraft would then move away from the small body once the sampling tool has acquired the sample. An active joint in the middle of the boom would then be activated to move the sampling tool to the spacecraft for transfer of sample to the spacecraft.

Figure 15 shows the prototype flexible boom that has been fabricated to test the sampling concept. A brush wheel sampler sampling tool will be attached to the boom. A sandbox will be placed on a lift device that will be moved vertically and horizontally to simulate the motion of the small body relative to the spacecraft and sampling tool. The sampling tool on the end of the boom will acquire sample out of the sandbox as the sandbox moves vertically and horizontally.

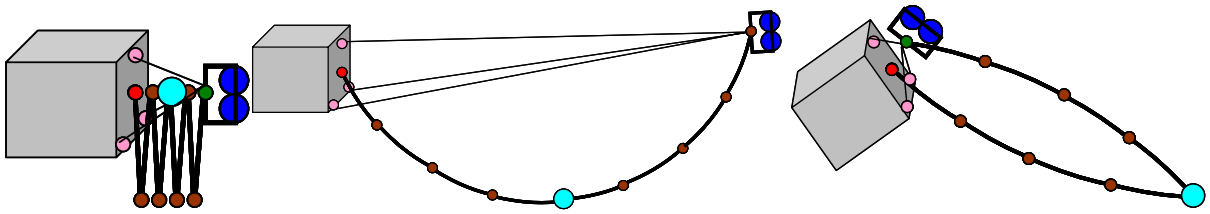

Figure 14. Deployable Flexible Segment Boom, stored before deployment, deployed for sampling, and retracted to the spacecraft for sample transfer.

Figure 15. Prototype DFS boom in the laboratory.

V. Conclusion

This paper has summarized the modeling, simulation, and testing work related to the development of technology to investigate the potential that shape memory actuation has to provide mechanically simple and affordable solutions for delivering assets to a surface and for sample capture and return. We investigate the structural dynamics and controllability aspects of an adaptive beam carrying an end-effector which, changing equilibrium phases is able to actively decouple the end-effector dynamics from the spacecraft dynamics during the surface contact phase. Asset delivery and sample capture and return are at the heart of several emerging missions to small bodies, such as asteroids, and to the surface of large bodies, such as Titan.

Acknowledgments

This research was carried out at the Jet Propulsion Laboratory, California Institute of Technology, under a contract with the National Aeronautics and Space Administration, and funded through the internal Research and Technology Development (RTD) program.

References

[1] Bayard, D. S. , Eisenman, D. : *Small Body Guidance, Navigation, and Control*, JPL Report D-36457, October 2006.
[2] Boyd, J.G., Lagoudas, D.C., *A Thermodynamical Constitutive Model for Shape Memory Materials. Part I. The Monolithic Shape Memory Alloy*, International Journal of Plasticity, Vol. 12, No. 6, pp. 805-842, 1996.
[3] COMSOL Multiphysics: User's Guide, Version 3.5a, COMSOL AB, November 2008.
[4] Dano, M.-L., Hyer, M. W., *SMA-Induced Snap-Through of Unsymmetric Fiber-Reinforced Composite Laminates*, International Journal of Solids and Structures, Vol. 40, pp. 5949-5972, 2003..
[5] Birman, V., *Review of Mechanics of Shape Memory Alloy Structures*, Applied Mechanics Reviews, Vol. 50, No. 11, Pt. 1, November 1997.
[6] Franzen, M.A., and Sears, M.A.: *The HERA Near-Earth Asteroid Sample Return Mission: an Overview*, Lunar and Planetary Science XXXIV (2003).
[7] Higuchi, K., Kawaguchi, J., Fujiwara, A., Okudaira, T., Yajima, S.: *Asteroid Sampling Mechanisms for MUSES-C*, NASA CP-2002/211505, Proceedings of the 36th Aerospace Mechanisms Symposium, Glenn Research Center, May 15-20, 2002.
[8] Massad, J.: *Macroscopic Models for Shape Memory Alloy Characterization and Design*, NCSU PhD Thesis, June 2003.
[9] Peffer, A., Fosness, E., Carpenter, B., and Denoyer, K., *On-Orbit Experiments and Applications of Shape Memory Alloy Mechanisms*, in Smart Structures and Materials 2000: Industrial and Commercial Applications of Smart Structures, Jack H. Jacobs, Editor, Proceedings of SPIE Vol. 3991 (2000).
[10] Seelecke, S., Muller, I.: *Shape Memory Alloy Actuators in Smart Structures: Modeling and Simulation*, Applied Mechanics Reviews, vol. 57. no.1, January 2004.
[11] Wayman, C.M., *Shape Memory and Related Phenomena*, Progress in Materials Science, Vol. 36, pp. 203-224, 1992.